2D3C Measurement of velocity, pressure and temperature fields in a intake flow of an air turbine by Filtered Rayleigh Sattering (FRS) and Validation with LDV and PIV

Michael Dues[1,*], Fritz Dues[1], Sergey Melnikov[1], Jonas J. Steinbock[1],Ulrich Doll[2],Ingo Röhle[3], Matteo Migliorini[4], Pavlos Zachos[4]

1: ILA R&D GmbH, Jülich, Germany
2: Aarhus Universitet (AU), Aarhus, Denmarky
3: Berliner Hochschule für Technik (BHT), Berlin, Germany
4: Cranfield University (CU), Cranfield, United Kingdom

*Corresponding author: dues@ila-rnd.de

Keywords: FRS, Seeding free, Fiber Optic, LDA, PIV.

ABSTRACT

A Filtered Rayleigh Scattering Technique is implemented in two different experimental setups and compared to the established velocity measurement techniques Laser Doppler Anemometry (LDA) and Particle Image Velocimetry (PIV). The Frequency Scanning Filtered Rayleigh Scattering Method employed uses an imagefiber bundle which allows for the simultaneous observation of the flow situation from six independent perspectives, utilizing only one sCMOS camera. A testrig with a nominal diameter of 80 mm was implemented by ILA R&D GmbH. Here measurements with straight pipe flow and a swirl generator were realised, as well as comparisions with LDA. A second experiment utilized Cranfields University's Complex Intake Facility (CCITF), enabling the simulation of the flow field for an engine intake as observed behind an S-Duct diffuser. The diameter in the measuring plane was 160 mm. Measurements up to a mach number of 0.4 were performed and compared with HighSpeed Stereo-PIV (S-PIV) measurements. Good agreement was achieved in respect to both the absolute magnitude of the velocity measurements as well as to the resolution of complex flow structures. The developed FRS multi-view Setup is able to simultaneously determine the 3D velocity components, the pressure and the temperature on a measurement plane with high resolution and without seeding. After calibration the FRS system yields the pressure and temperature within 3 percent respectively 0.8 percent of the reference values. The measured velocity was within 1-2 m/s of the reference.

1. Introduction

The reduction of fuel consumption and emissions plays a key role in the development of new aircraft concepts. In this context, new concepts are being developed that integrate the engines into the aircraft body (Kim et al. (2013)). This causes, for example, disturbed stationary and unsteady inflows to the engines due to boundary layer flows, which significantly influence their aerodynamic load and operating behavior (Doll, Migliorini, et al. (2022)). To investigate such inlet disturbances,

grids with total pressure probes have often been used to investigate velocity and pressure distributions (SAE International (2017)), but their spatial and temporal resolution is limited in terms of their ability to resolve the flow structures that occur and they are not without repercussions on the flow itself. There is therefore a need for measurement methods that are as unintrusive as possible and allow the simultaneous recording of velocity, pressure and temperature fields in engine intakes. A measurement method that does not require the addition of seeding into the flow would be of great advantage in order to be able to carry out such inlet disturbance investigations not only in test bench tests, but also potentially in flight tests.

The EU research project SINATRA "Seeding free non intrusive aero engine distortion measurements" is therefore investigating the possibility of using the Filtered Rayleigh Scattering technique (FRS) for the seeding-free investigation of inlet flows in engines on the test bench and potentially in flight tests. FRS measurements are first carried out on a simplified flow experiment in order to optimize the test setup, characterize the measurement system and determine the measurement uncertainty. In a second step, FRS measurements of the pressure and velocity field are then carried out on a test rig resembling engine intakes at Cranfield University.

This article describes the structure of the measurement system, the simplified test rig at the ILA and the test rig for investigating inlet flows at Cranfield University. In a first step, the FRS measurements are validated on the simplified test setup using detailed LDA measurements on an undisturbed pipe flow. Subsequently, various swirl flows are investigated using FRS with regard to velocity, pressure and temperature distribution. Finally, the results of the FRS measurements at the test stand in Cranfield are discussed in comparison to PIV measurements.

2. Measurement principle

The frequency scanning method for FRS (FSM-FRS) is based on the evaluation of the Rayleigh scattering of the laser light on the gas molecules in the flow. The Rayleigh scattering occurring at the gas molecules has a spectral distribution of several GHz width and contains information about temperature, pressure, velocity and density in the illuminated measuring range. However, reflections of laser light on walls (geometric scattering) or on particles (Mie scattering) are not broadened in frequency and can be filtered out of the measurement signal with the aid of a molecular filter, in this case an iodine cell. A schematic of the scattering process can be found in Fig. 1 (left), the principle of frequency scanning is drawn in Fig. 1 (right).

The light scattered by the molecules is imaged by the iodine cell onto a camera sensor and transferred into an intensity value. However, the spectral information on temperature, pressure, density and speed is lost as a result. In accordance with the FSM-FRS method further developed by DLR Cologne, the frequency of the laser system is therefore varied in discrete steps along the filter curve of the iodine cell so that an intensity curve is created for each pixel depending on the laser

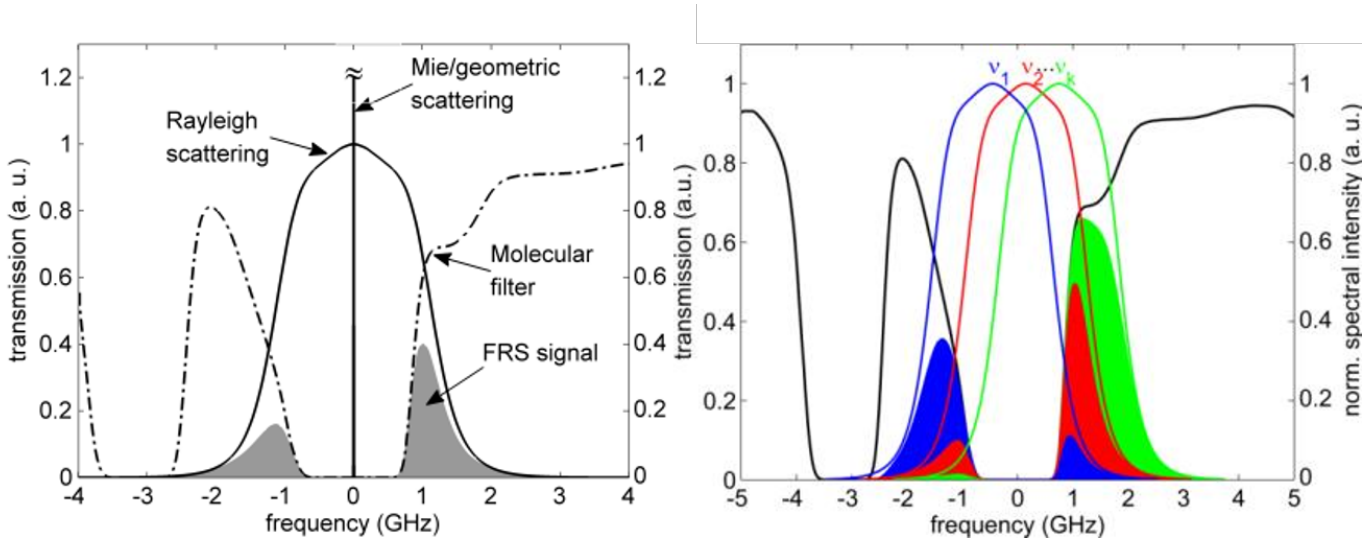

Figure 1. Left: The Rayleigh-scattered light from the narrow-band laser at the fluid molecules is filtered with an iodine cell, which removes reflections from surfaces and scattering from large particles (Mie scattering). Right: Frequency scan method: The laser frequency is shifted along the transmission profile of the molecular filter. Time-averaged pressure, temperature and velocity fields (Doppler shift) can be determined simultaneously from the resulting intensity spectra. The observing camera will detect the integrated convolution between the Rayleigh Spectra and the transmission curve of the iodine cell.

frequency. The temperature, pressure, speed and density can be reconstructed from this intensity curve using a suitable measurement model (Doll et al. (2018)).

The FRS system consists of the components frequency-controlled laser, light section probe, light arm, camera module with iodine cell and CMOS camera as well as a multi-arm image guide with lenses. In order to allow simultaneous determination of three velocity components, the pressure and the static temperature, the measurement cross-section is viewed from six perspectives and imaged onto the sensor of a single camera.

3. Validation experiments in a simple flow configuration

3.1. Lab scale test rig at ILA R&D GmbH

The simplified test setup (Fig. 2 and 3) essentially consists of a conditioned pipe in whose measuring cross-section with an internal diameter of 80 mm flow velocities of up to 100 m/s can be generated. Optical access granted is via an anti-reflective coated glass tube. The light sheet is coupled in via a bespoke airtight slit in the pipe.

Figure 4 displays the unifying image fiber bundle used to observe the flow from six perspectives. The active area on the inlet of each of the six fiber arm is 4x4 mm with about 50000 individual fibers. The inlet of each 3 m fiber arm is equipped with an adjustable fiber objective. The outlet of the

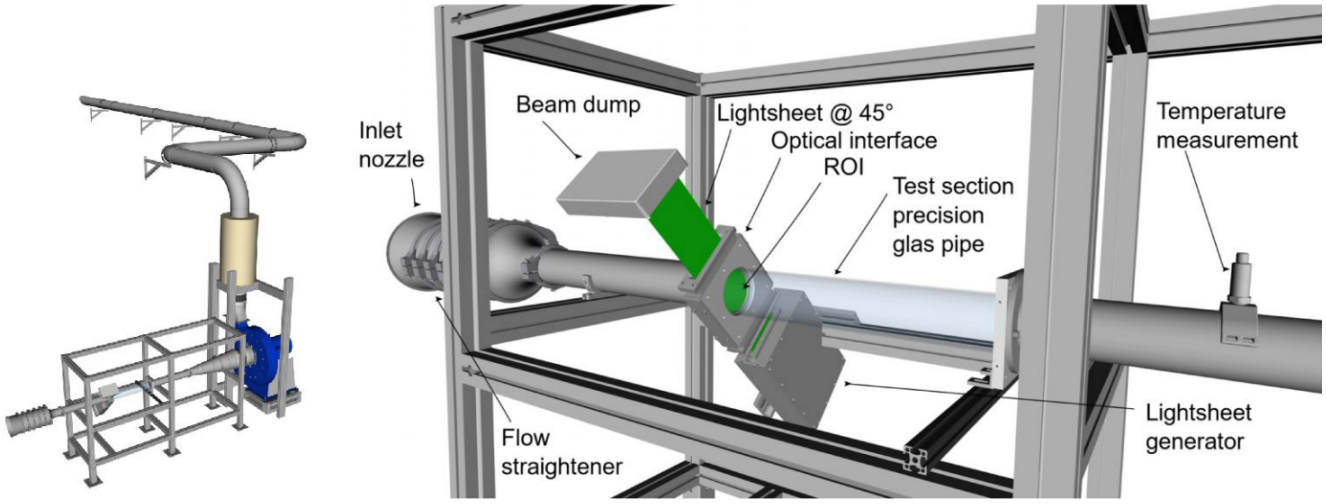

Figure 2. Rendering of ILA R&D GmbH's test rig for the analysis of pipe flows. Testrig including piping, the overall length of the piping is 15 m (left). Measuring section with calibrated glas duct at the ROI, the inner diameter is 80 mm (right).

fiber bundle has an active area of 12x8 mm, thus allowing to capture 6 perspectives with only one camera module. This setup allows for measurements in environmental challenging environments: the delicate camera module can be placed in a protected location up to 3 m away from the object. The fiber heads are mounted on adjustable magnetic lab stands, allowing for fast alignment and adaption of perspectives according to the experimental requirements. The optical setup results in an optical resolution of about 1 mm in the ROI for the depicted setup.

The outlet of the fiber bundle is attached to a bespoke camera module consisting of a temperature stabilized molecular filter (iodine cell) and an pco.edge 4.2 sCMOS camera with a resolution of 2048x2048 pixel for aquiring the image data.

The observation perspectives for the experiments have been selected according to the optimization frame work developed byDoll, Röhle, & Dues (2022) and Doll, Röhle, Dues, & Kapulla (2022).

Due to the inlet configuration consisting of flow straightener, a contraction and a relatively short distance to the measuring cross-section, a fully developed pipe flow profile is not available at the region of interest (ROI). Instead a 'flat-top' profile is expected. To validate the FRS measurements, the velocity field in the pipe is recorded on a dense grid for three operating points using a calibrated Laser Doppler Velocimetry (LDV).

3.2. Validation of the velocity measurements with Laser Doppler Anemometry

Figure 5 shows the velocity profile (c) measured with FRS for three operating points in comparison to the velocity profiles measured with LDV (Doll et al. (2023)). In the center region of the

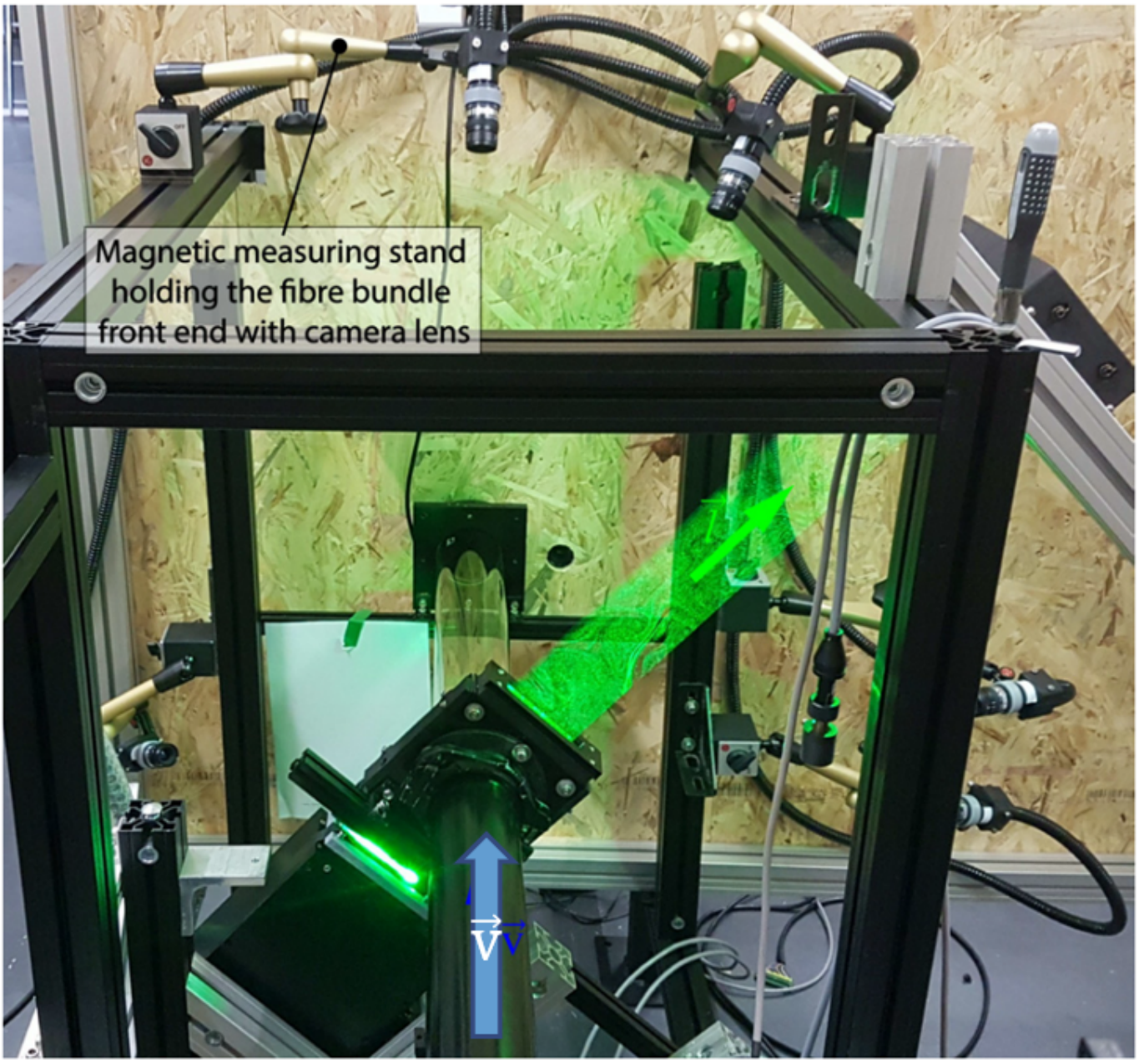

Figure 3. Overview of the the six fiber cameras arranged around the measurement Plane Region of Interest (ROI).

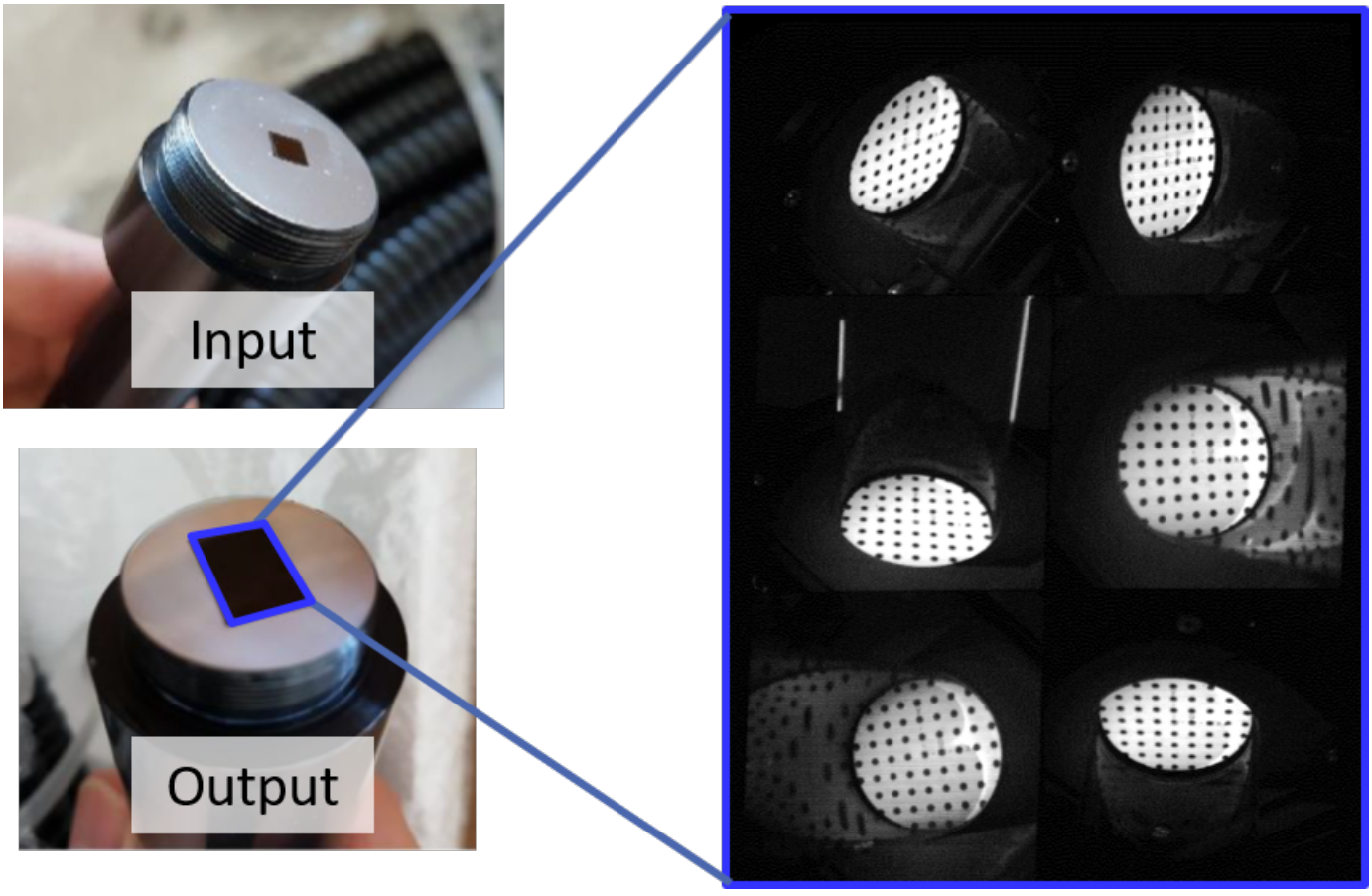

Figure 4. Input and output view of the six to one imagefiber bundle used to oberserve the scene simultaneously from different perspectives (left). Resulting image for observation of a calibration target (right).

flow, the flow profile is strongly flattened in both the LDV and FRS measurements, while a flow gradient occurs in the edge region due to the boundary layers that build up. In the center area, the difference between the FRS and LDV measurements is less than 1more sharply, but this can be explained by the measurement position of the LDV measurement further downstream. The static pressure (a) measured using FRS corresponds very well with the integral comparative pressure measured behind the nozzle. The same applies to the FRS-based temperature (b) in comparison to the isentropic calculated reference temperature in the flow cross-section.

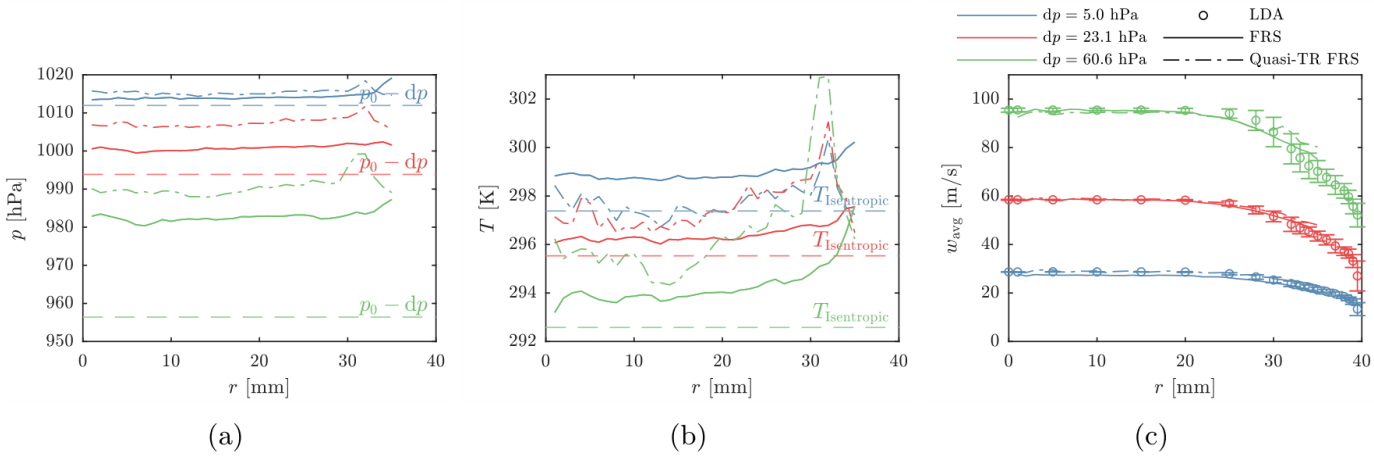

Figure 5. Comparision of the FRS-derived values for pressure (a), isentropic temperature (b) and axial velocity with the reference values provided by the test rig, resp. LDA measurements.

4. Application on a complex flow field

To test the applicability on a more complex flow field a swirl generator was installed upstream of the ROI in the test rig. The geometry of the swirl generator is depicted in Figure 6. The swirl generator consists of two regions. An inner region featuring 4 screwed guide vanes used to impose a swirl motion on the center portion of the axial flow. The outer region is equipped with 4 axial guide vanes to minimize swirl in the proximity of the pipe wall. The swirl generator has been manufactured using resin printing.

Figure 7 shows the measured 3C velocity distribution approximately 20mm behind the swirl generator for the three operating points 30 m/s, 60 m/s and 100 m/s. For all operating points, the circumferential components of the velocity in the secondary flow can be clearly recognized. The circumferential components are strongest in the region of $r/R \approx 0.5$, declining towards the center and the walls. The wake dents of the four swirl vanes are clearly visible, especially in the distribution of the axial component w. In the center of the vortex a small backflow region is visible.

Figure 8 shows the measured 3C velocity distribution approximately 70mm behind the swirl generator for the three operating points 30m/s, 60 m/s and 100m/s. In comparision to Fig. 7 the swirl

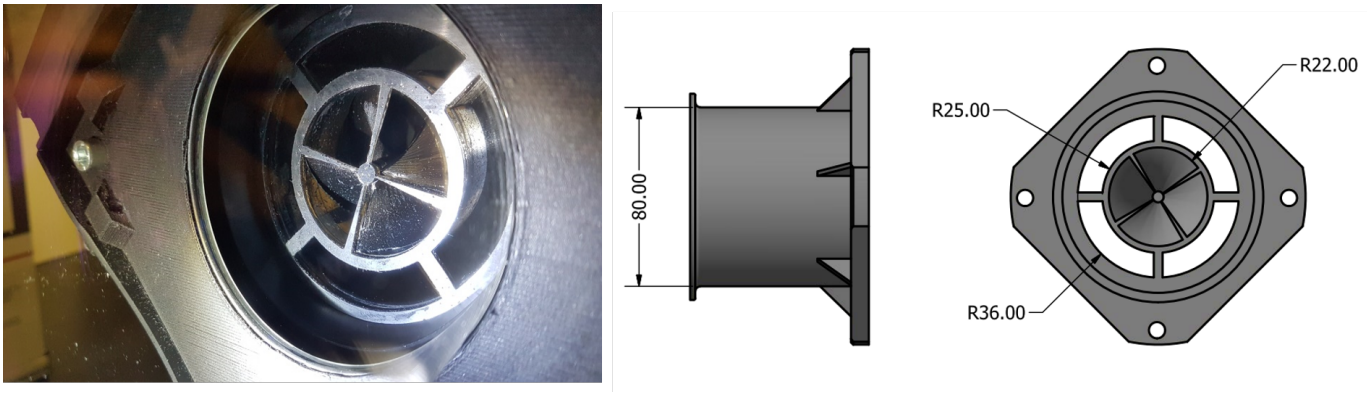

Figure 6. Swirl generator: Installed in the test rig (left). CAD rendering (right). The swirl generator is installed in two configurations: 20 mm and 7D upstream of the ROI.

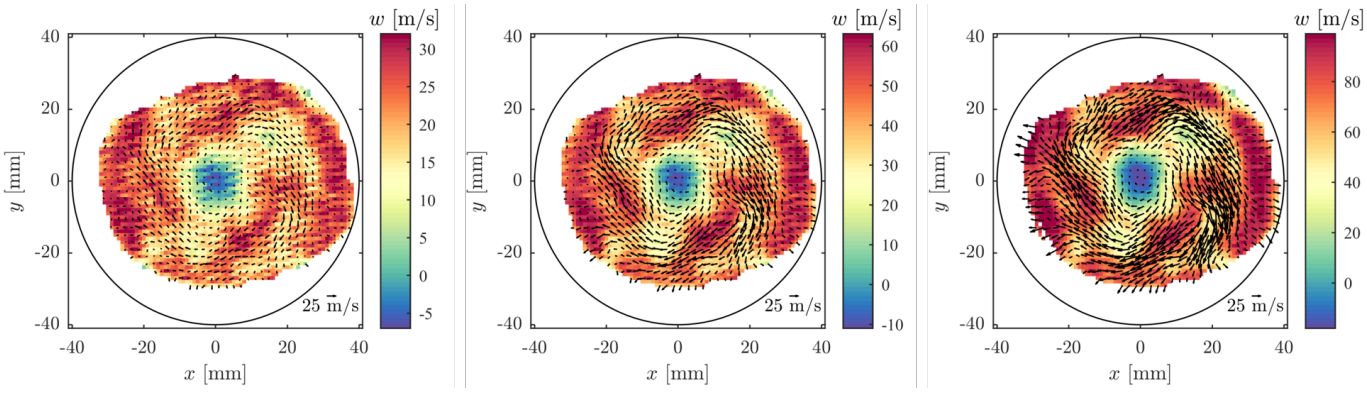

Figure 7. Velocity distribution with the swirl generator installed 20 mm upstream of the ROI. For nominal flow velocities of 30 m/s (left), 60 m/s (center) and 100 m/s (right). The axial velocity is color coded according to the colormap on the right side of each plot. The in-plane velocities are overlayed with arrows.

developed more evenly and is no longer confined to the central region. The wakes of the guide vanes are no longer visible.

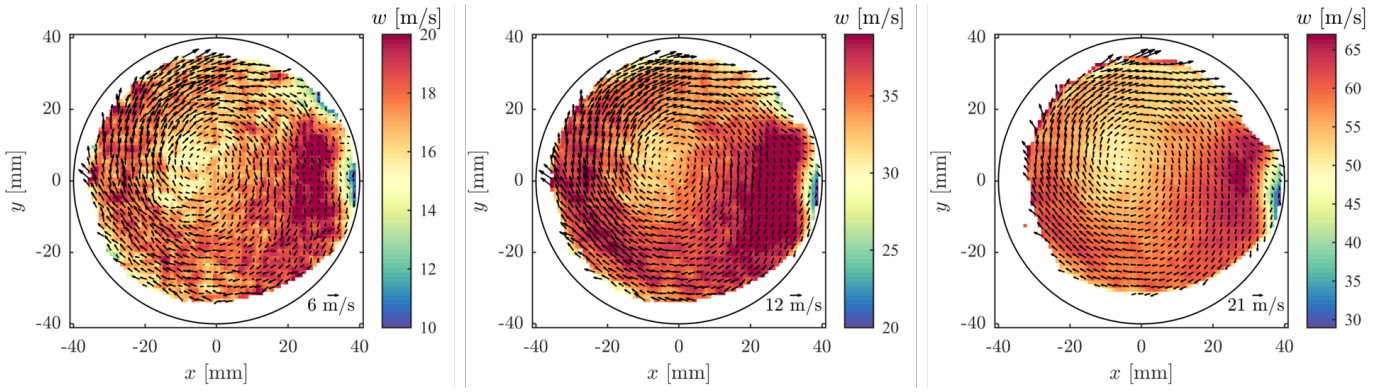

Figure 8. Velocity distribution with the swirl generator installed 70 mm upstream of the ROI. For nominal flow velocities of 30 m/s (left), 60m/s (center) and 100m/s (right). The axial velocity is color coded according to the colormap on the right side of each plot. The inplane velocities are overlayed with arrows.

To test the FRS temperature measurement, a hot air flow was fed at a comparatively low speed into one of the swirl ducts, compare Fig. 9. At the inlet of the glas tube a hot gun was placed which generated the hot streak.

Figure 9. Glas tube inserted in one of the channels of the swirl generator for insertion of a hot flow streak. The cables sleaves visible are for a temperature sensor mounted at the tip of the glas tube(left). Inlet configuration for hot streak measurments with glas tube inserted in one of the channels of the swirler (right).

The resulting temperature field is depicted in Fig. 10. The localized hot streak resulting from the insertion of the hot air flow is clearly visible at all flow velocities. Relative temperature differences in the order of 1 Kelvin resolved.

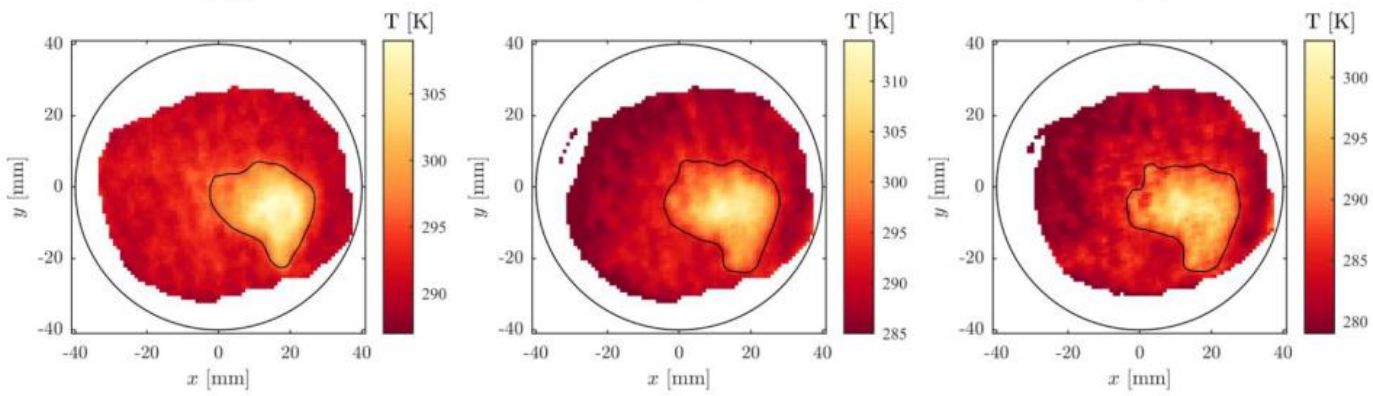

Figure 10. Temperature distribution measured by FRS behind a hot temperatur streak inserted in one of the swirl generators channels. Nominal velocity 30 m/s (left), 60 m/s (center) and 100 m/s (right).

The lower axial velocity as depicted in Fig. **??** due to the blockage of the injecting glass tube and the insertion of a smaller velocity hot flow is reflected in the diminished outflow of a segment of the swirl generator. The drawn contour corresponds to the zone of increased temperature due to the hot gas injection in Fig. 10.

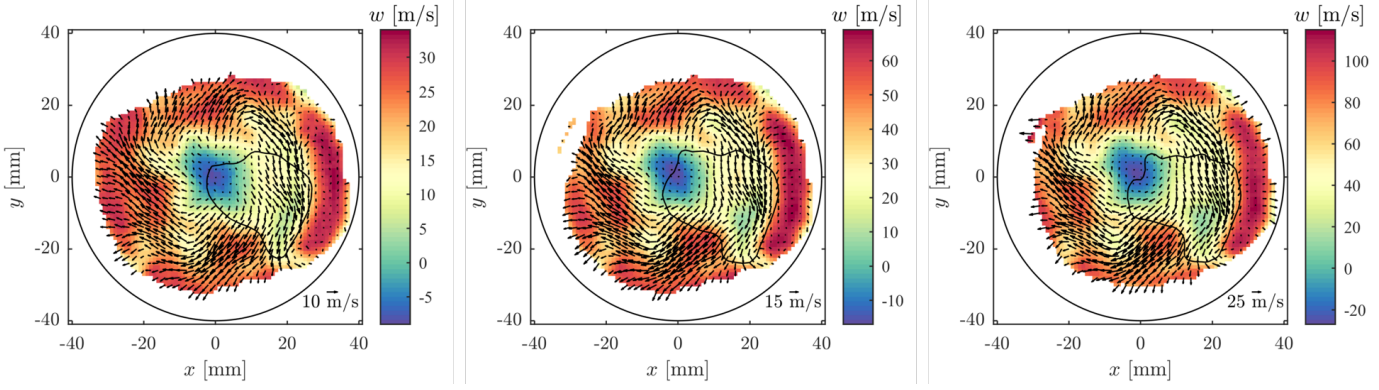

Figure 11. Velocity distribution with the swirl generator installed 20 mm upstream of the ROI. For nominal flow velocities of 30 m/s (left), 60 m/s (center) and 100 m/s (right). The axial velocity is color coded according to the colormap on the right side of each plot. The inplane velocities are overlayed with arrows. The black overlay is the region of the hotstreak.

The lower axial velocity is also reflected in the derived pressure fields, compare Fig. 12. The region affected by the insertion of the hot streak (one channel of the swirl generator) features a lower static pressure.

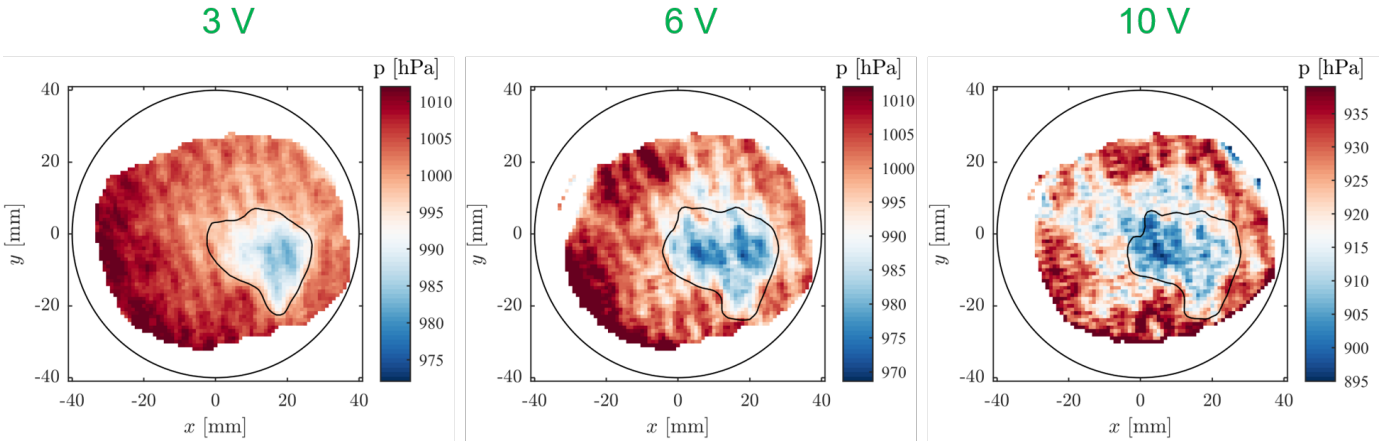

Figure 12. Pressure distribution measured by FRS behind a hot temperatur streak inserted in one of the swirl generators channels. Nominal velocity 30 m/s (left), 60 m/s (center) and 100 m/s (right).

4.1. Complex Intake flow setup

The Cranfied Complex Intake Test Facility (CCITF) provides a experimental platform for the analysis of engine intakes. It is capable of producing internal flows up to a Mach number of 0.6. In frame of the SINATRA project a "high-offset" S-Duct diffuser configuration was choosen as reference experiment. More Information on the CCITF can be found in Migliorini et al. (2024). A overview about the geometric setup is given in Figure 13.

The internal diameter of the optical test section is 160 mm. The measurement plane was placed close to the outlet of the S-Duct. A bespoke light sheet interface enabled the illumination of the ROI with the laser. The available light sheet could illuminate approximately half of the cross section, therefore each experiment was conducted once with the lightsheet traversed to the respective upper and once traversed to the lower part of the ROI, compare Figure 14. The FRS measurements where then evaluated for each part, the resulting fields were stitched together via software.

During the FRS measurement campaign the following flow conditions where examined: 0.18, 0.27 and 0.4 Mach at the ROI. The resulting velocity fields are depicted in Fig. 15. The axial velocity profile is skewed with higher velocities on the right side of the ROI due the s-duct inlet. The formation of the secondary flow (dean vortices) is clearly observable. About 80independently from 6 perspectives. Due to the multi image-fiber approach it is possible to observe almost the entire crossection with multiple perspectives, thus allowing for robust measurements even though some regions are inherently blocked or shaded due to experimental constraints on individual fiber

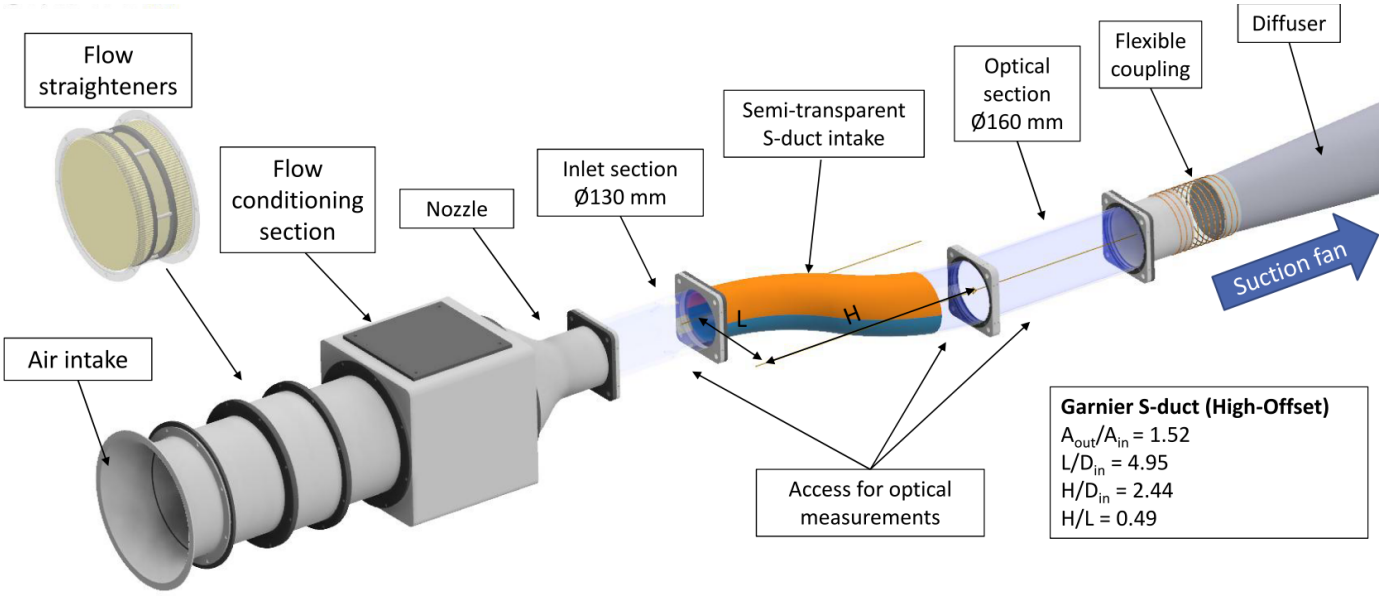

Figure 13. Rendering of the Cranfield Complex Intake Test facility (CCITF).

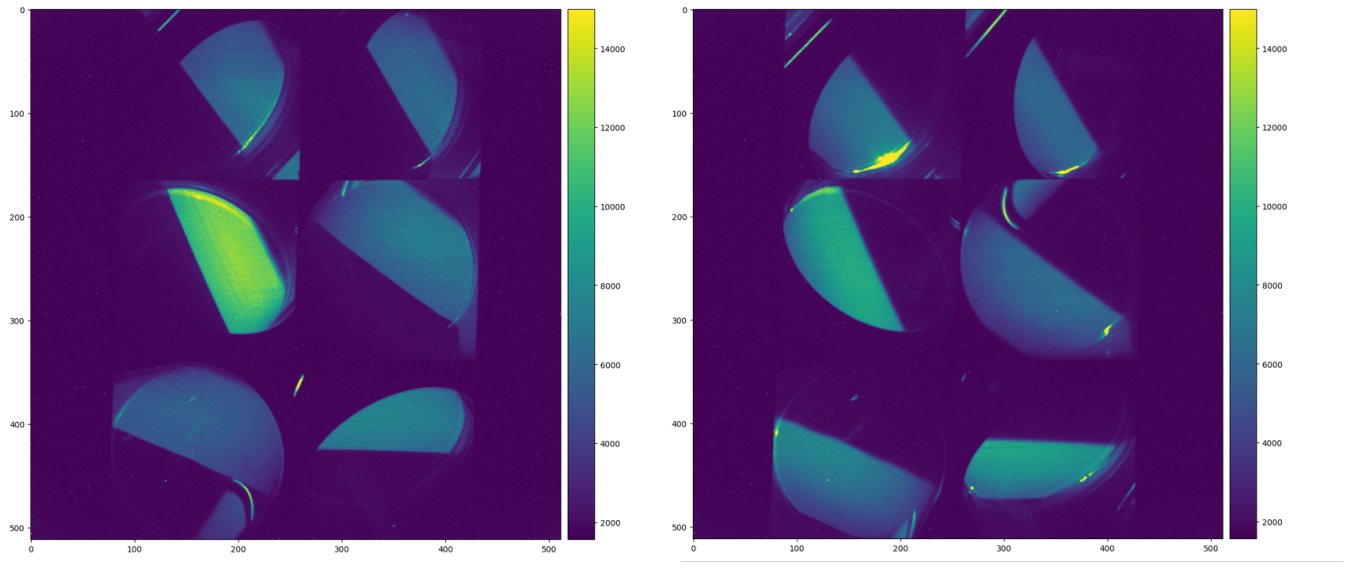

Figure 14. Illumination of the upper (left) and lower part of the ROI (right) by the traversed lightsheet as observed by the image fiber bundle.

heads.

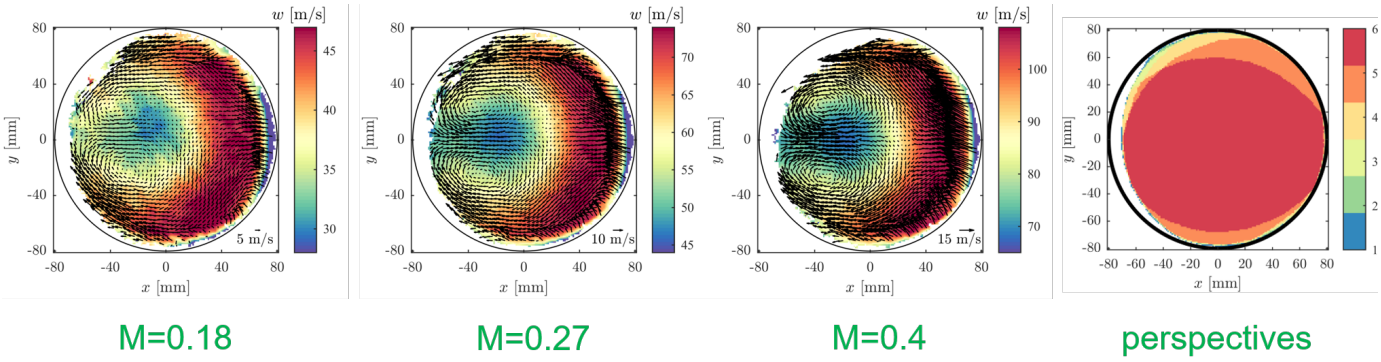

Figure 15. Axial velocity field obtained with FRS at the CCITF at 0.18 Mach (left), 0.27 Mach (center left) and 0.4 Mach (center right). The in-plane components are denoted with black arrows. The number of valid perspectives is drawn as insert (right).

4.2. Comparison with time-averaged Particle Image Velocimetry Measurements

A measurement campaign with time-averaged Stereo Particle Image Velocimetry (S-PIV) was conducted by Cranfield University to generate benchmark data for the FRS velocity measurements. The S-PIV system used two SCMOS cameras with a resolution of 1280 by 800 pixel at 8 kHz. The resulting spatial resolution in the ROI is in the order of 2.3 mm. DEHS seeding with an nominal diameter of 1 μm was illuminated by an pulsed ND:YAG laser. 20000 flow-fields were captured and averaged to create the reference data set.

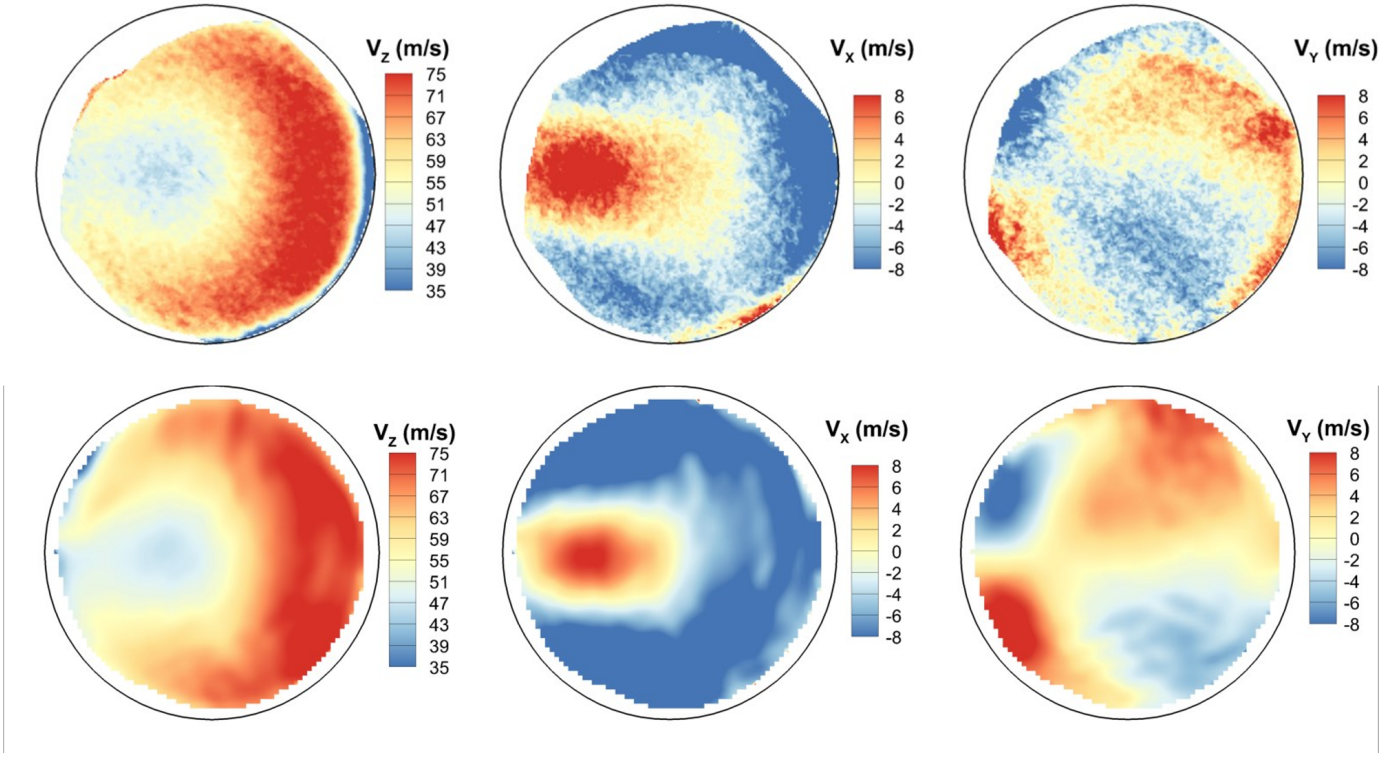

Figure 16. Time-averaged distribution maps of the 3D velocity field measured by FRS at the AIP of the CCITF for a Machnumber of 0.27 (top). Time-averaged distribution maps of the 3D velocity field measured by PIV (bottom).The averaging is done for 20'000 timesteps for PIV.

5. Summary

A Frequency Scanning multiview FRS Setup has been built up and compared to established measurement techniques. For the measurement of the velocity deviations from the reference in the order of 1-2 m/s absolute were accomplished.

For the pressure and temperature the FRS measurements yields the reference value within 3% respectively 0.8%. Furthermore it was observed that robust measurements in the proximity of the wall were achieved, due to the effective suppression of the Mie Signal and the Multi-Perspective redundancy.

The flow, temperature and pressure field behind a swirl generator is measured and discussed.

An mockup of an intake flow has been measured using FSM-FRS and PIV. The complex flow fields were resolved and yield very good agreement.

The presented multiview FSM-FRS is deemed suitable for high-velocity measurements were seeding is not possible or very difficult with the added value of simultaneous high spatial temperature and pressure measurement.

Acknowledgements

This project has received funding from the Clean Sky 2 Joint Undertaking (JU) under grant agreement No 886521. The JU received support from the European Union's Horizon 2020 research and innovation programme and the Clean Sky 2 JU members other than the Union.

References

Doll, U., Dues, M., Bacci, T., Picchi, A., Stockhausen, G., & Willert, C. (2018, sep). Aero-thermal flow characterization downstream of an NGV cascade by five-hole probe and filtered Rayleigh scattering measurements. *Experiments in Fluids*, *59*(10). Retrieved from https://elib.dlr.de/121918/3/PrePrint-Doll-2018-ExiF59-150-s00348-018-2607-z.pdf doi: 10.1007/s00348-018-2607-z

Doll, U., Kapulla, R., Steinbock, J. J., Dues, M., Migliorini, M., & Zachos, P. K. (2023). Seeding-free inlet flow distortion measurement by filtered Rayleigh scattering: diagnostic approach and verification. *AIAA SciTech Forum*. Retrieved from https://arc.aiaa.org/doi/pdf/10.2514/6.2023-1372 doi: 10.2514/6.2023-1372

Doll, U., Migliorini, M., Baikie, J., Zachos, P. K., Röhle, I., Melnikov, S., ... Lawson, N. J. (2022, apr). Non-intrusive flow diagnostics for unsteady inlet flow distortion measurements in novel aircraft architectures. *Progress in Aerospace Sciences*, *130*, 100810. doi: 10.1016/j.paerosci.2022.100810

Doll, U., Röhle, I., & Dues, M. (2022, 07). Unsteady multi-parameter flow diagnostics by filtered rayleigh scattering: system design by multi-objective optimisation. In *20th international symposium on the application of laser and imaging techniques to fluid mechanics.* Retrieved from https://www.researchgate.net/publication/362067961_Unsteady_multi-parameter_flow_diagnostics_by_filtered_Rayleigh_scattering_system_design_by_multi-objective_optimisation

Doll, U., Röhle, I., Dues, M., & Kapulla, R. (2022, July). Time-resolved multi-parameter flow diagnostics by filtered rayleigh scattering: system design through multi-objective optimisation. *Measurement Science and Technology*, *33*(10), 105204. doi: 10.1088/1361-6501/ac7cca

Kim, H. D., Felder, J. L., Tong, M. T., & Armstrong, M. (2013). Revolutionary aeropropulsion concept for sustainable aviation: Turboelectric distributed propulsion. Busan, Korea. Retrieved from https://ntrs.nasa.gov/api/citations/20140002510/downloads/20140002510.pdf

Migliorini, M., Zachos, P. K., MacManus, D., Doll, U., Dues, M., Steinbock, J., ... Röhle, I. (2024). Seeding-free inlet flow distortion measurements using filtered rayleighscattering: integration in a complex intake test facility. *AIAA Conference (submitted)*. Retrieved from https://arc.aiaa.org/doi/abs/10.2514/6.2024-2831 doi: 10.2514/6.2024-2831

SAE International. (2017, April). Gas turbine engine inlet flow distortion guidelines. *AEROSPACE Standard ARP 1420C*. Retrieved from https://saemobilus.sae.org/content/arp1420c doi: 10.4271/arp1420c